The 9th European Congress on Computational Methods in Applied Sciences and Engineering
ECCOMAS Congress 2024
3 – 7 June 2024, Lisboa, Portugal

COMPETITIVENESS OF COMPUTATIONAL MODELLING STRATEGIES: A FRAMEWORK TO IMPLEMENT EFFICIENT DIGITAL TWINS OF HISTORICAL MASONRY STRUCTURES

ANNALAURA VUOTO[1], MARCO F. FUNARI[2], SIMON SZABÓ[1], BORA PULATSU[3], AND PAULO B. LOURENCO[1]

[1] ISISE Department of Civil Engineering, University of Minho Campus de Azurém, Guimarães, Portugal, annalauravuoto1307@gmail.com, simon.szabo117@gmail.com, pbl@civil.uminho.pt

[2] School of Sustainability, Civil and Environmental Engineering, University of Surrey, UK, m.funari@surrey.ac.uk

[3] Department of Civil and Environmental Engineering, Carleton University, Ottawa, Canada, bora.pulatsu@carleton.ca

Keywords: Digital Twin, Unreinforced masonry (URM), computational modelling.

Summary. *This paper proposes a framework for implementing rational digital twins for the structural integrity historic masonry structures by examining the competitiveness and reliability of various computational strategies. To this end, the structural behaviour of an unreinforced masonry pier-spandrel system is analysed using the discrete element method and reduced discrete rigid block analysis. Additionally, the finite element method, in which masonry is modelled as a homogeneous continuum incorporating continuum discretisation with a plasticity-based damage model, is also considered. Analytical approaches based on limit analysis, including both micro and macro-LA, are hence explored. Comparisons among the computational modelling strategies are performed by analysing computational efficiency and the accuracy of the response measures predicted.*

1 INTRODUCTION

Structural integrity protection of Built Cultural Heritage (BCH) poses challenges that demand innovative approaches [1]. Computational modelling is a crucial component of the Digital Twin (DT) paradigm, which has emerged as a promising concept across industries, enabling real-time monitoring, predictive maintenance, and improved decision-making. A DT is a digital replica of a physical asset, simulating performance under various conditions [2], [3]. DT concept is domain-specific, with varying definitions depending on field requirements. In BCH conservation and related fields, developing DTs is costly due to the need for high-precision data, significant computational resources, and complex modelling while also considering the intangible cultural value of the assets, necessitating a balance between model accuracy and economic feasibility [4].

This paper proposes a DT framework tailored for BCH conservation (Section 2), featuring a non-continuous updating strategy triggered by significant changes in the asset's condition to optimise resource use. The framework aims to predict unreinforced masonry (URM) structures'

structural performance, balance model accuracy with cost-effectiveness, and provide a structured approach for BCH conservation, respecting historical and practical conservation constraints. This manuscript focuses on the first steps of the proposed methodology (Sections 3-4) and critically discusses their outcomes (Section 5).

2 STRUCTURAL MODEL UPDATING FRAMEWORK FOR HERITAGE BUILDINGS

Creating accurate structural models of heritage structures is costly and computationally intensive. This study proposes a DT framework, theoretically introduced by Vuoto et al. in [5], to predict BCH structural performance by optimising the trade-off between model reliability and associated costs. The process of assessing the structural performance of URM structures involves i) inspection and diagnosis phase to achieve a certain Level of Information (LoI); and ii) development of a numerical model with a defined Modelling Refinement (MR). The goal of the proposed framework is to find an optimal combination of LoI and MR to achieve accuracy and computational efficiency by refining the model based on evidence obtained via non-destructive testing. The development of the framework involves the following steps:

0. Physical Asset (PA) collection information.
1. Digital Assets (DAs) numerical modelling: tuning of MR (see Section 4).

The PA modelling can be performed using different approaches here named as DAs, e.g. MR1) Discrete Element Modelling (DEM), MR2) Finite Element Modelling (FEM), MR3) Micro Limit Analysis (Mi-LA), and MR4) Macro Limit Analysis (Ma-LA), each characterised by a decreasing level of refinement and computational cost.

2. DAs numerical modelling: tuning of LoI.

Different LoIs can be achieved and defined according to various data acquisition strategies. Theoretically, the less testing and information are available, the more inaccuracy of the of numerical model increases. At this stage, a proper cost analysis should be performed for each LoI. Each iteration will allow users to work with more data and fewer uncertainties, enabling them to adopt more refined numerical models.

3. DAs model reliability evaluation.

For each model refinement, the scatter of the response measure must be evaluated. Once the solution's convergence is achieved, the iterations/refinements can be stopped. A graphical representation of the proposed framework is presented in [5].

It is worth pointing out that in this paper, we focus only on the comparison of different MRs to measure model reliability compared to a Simulated Physical Asset, which is described in the following section.

3 SIMULATED PHYSICAL ASSET

A pier-spandrel system tested under in-plane lateral loading by Augenti et al. [6], [7] was selected. This system (Figure 1) served as the PA for creating its digital counterpart. A Simulated Physical Asset (SPA) was built and used as a benchmark model. In the following section of the manuscript, we will refer to the SPA as a representative of the PA to compare the performance of the other DAs.

A numerical approach using discontinuum-based modelling, labelled Discrete Rigid Block Analysis (D-RBA), was employed to develop the SPA [8] (Figure 1 (a,b)). It uses geometrical

properties from the experimental test (Figure 1 (a)), and mechanical properties based on mechanical tests performed by Augenti and Parisi [9], [10]. The SPA model's parameters are listed in Table 1 and they represent the reference dataset of mechanical properties for all the numerical approaches (MRs)) employed as follows.

Table 1: Linear and non-linear contact properties (SPA dataset)

BLOCKS

E_b [GPa]	G_b [GPa]	$f_{t,b}$ [MPa]	$k_{n,b}$ [GPa/m]	$k_{s,b}$ [GPa/m]	c_b [MPa]	$\varphi_{0,b}$ [°]	$\varphi_{res,b}$ [°]	$G^I_{f,b}$ [N/m]	$G^{II}_{f,b}$ [N/m]
1.54	0.44	0.23	10	4	0.46	38	38	8	550

MASONRY

w_M [kN/m^3]	v [-]	E_M [GPa]	G_M [GPa]	$k_{n,j}$ [GPa/m]	$k_{s,j}$ [GPa/m]	$f_{t,j}$ [MPa]	$c_{0,j}$ [MPa]	$c_{res,j}$ [MPa]	$\varphi_{0,j}$ [°]	$\varphi_{res,j}$ [°]	$f_{c,M}$ [MPa]
16	0.22	2.22	0.92	20	8	0.15	0.15	0.15	16.2	14.6	4.3

$G^I_{f,M}$ [N/m]	$G^{II}_{f,M}$ [N/m]	$G_{c,M}$ [N/m]
4.3	125	12800

b = blocks; M = masonry; j = joints

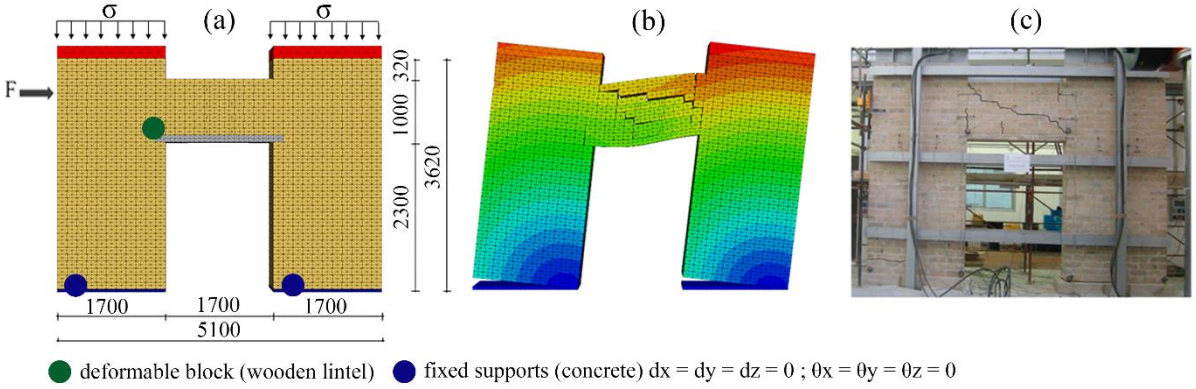

Figure 1: Pier-spandrel system [7]: (a) SPA D-RB model and specimen geometry; (b), (c) Validation of the SPA model against the PA (experimental test)

4 COMPUTATIONAL FRAMEWORK

This section details the development of step 1 of the framework. Four modelling techniques with were used to model the pier-spandrel system: MR1) DEM, MR2) FEM, MR3) Mi-LA, and MR4) Ma-LA. Sub-grades of refinement were introduced within MR1, MR2, and MR4, as described in the respective subsections. For each modelling technique, the theoretical background is briefly outlined.

4.1 Discrete Element Modelling (MR1)

The DEM, first introduced by Cundall [11], [12], [13], models interactions between rigid or deformable blocks (replicating masonry's discontinuity) using contact stress-displacement

laws, dynamically updating block velocities and positions until a quasi-static solution is reached. Different assumptions can be made within the DEM to simplify the complexity of the computational modelling. In this case, two sub-grades of refinement were introduced within MR1: MR1.1) Discrete Rigid Block Analysis with No Cracking Surface (D-RBA-NCS), and MR1.2) Reduced Discrete Rigid Block Analysis (RD-RBA).

In MR1.1, masonry units are modelled as rigid blocks with zero-thickness mortar joints, with blocks expanded by half the mortar thickness. Deformations occur only at the joints, and the equations of motion are integrated using the central difference method. This approach differs from the D-RBA used for modelling the SPA [8], where each masonry unit comprises two rigid blocks sharing a potential cracking surface (With Cracking Surface, D-RBA-WCS) (Figure 2 (a)). In MR1.1, block failure is not accounted for. This simplification reduces the required mechanical parameters from 25 to 15 (Table 4), also easing the modelling process in 3DEC and lowering computational demands. While the SPA required the implementation of two distinct contact surface categories (one for the mortar joints between the blocks, black in Figure 2 (a), and the other for the potential crack surface within the block, red in Figure 2 (a)), characterised differently from a mechanical standpoint, MR1.1 only requires the first (Figure 2 (b)). Characterisation of the contact models used is available in [8] and the properties employed are analogous to SPA (Table 1) for the masonry part only (subscript *M* in Table 1).

An alternative to existing macro-block methods within DEM, termed RD-RBA by Pulatsu et al. [14], is introduced as MR1.2. This approach reduces the computational cost and complexity of detailed models like D-RBA by using a limited number of rigid macro-blocks to represent the pier-spandrel system (Figure 2 (c)). The reduced D-RBA calculates the ultimate lateral load of the pier spandrel system for six predefined kinematic mechanisms [14], [15] using a Coulomb-slip joint model in shear, requiring cohesion and friction angle, while tensile strength is not defined. A bilinear behaviour with softening after reaching compression strength is considered for compression. Mechanical properties assumptions for modelling the RD-RBA are reported in [14].

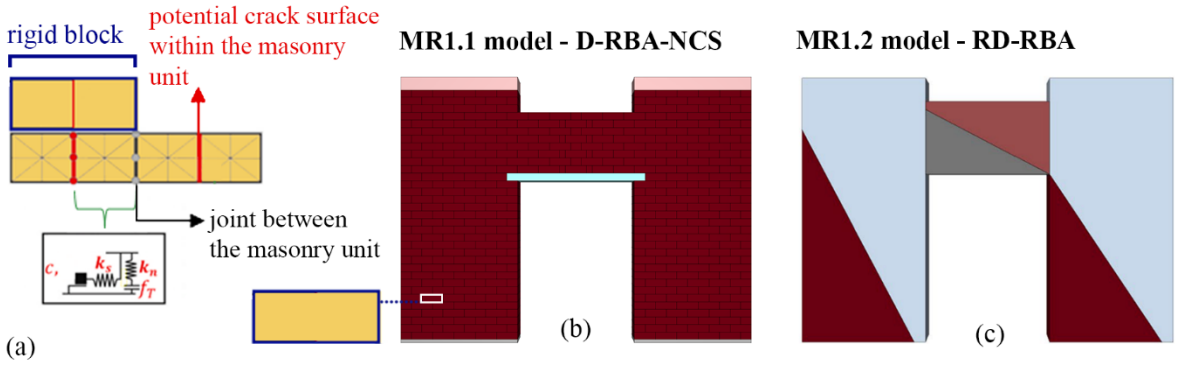

Figure 2: MR1 – Discrete Element Modelling. (a) Discretisation of the masonry unit in the SPA by introducing a potential cracking surface (D-RB-WCS model); (b) Detailed Rigid Block with No Cracking Surface (D-RB-NCS) model compared with (c) Reduced (RD-RBA) modelling

4.2 Finite Element Modelling (MR2)

The so-called macro-modelling approach is followed, meaning the masonry arrangement is smeared over a homogeneous material. This is particularly convenient for the analysis of large-scale structures [16], [17] since it offers the possibility to reproduce the macroscopic masonry mechanical behaviour through several models, e.g., the smeared crack concrete, the brittle crack concrete, and the concrete damage plasticity (CDP) models, here adopted. Specifically, CDP couples plasticity with a scalar-based damage model, and, as it was originally developed for concrete, an isotropic elastic behaviour is assumed. In the elastic regime, masonry is assumed to be deformable following an isotropic and linear elastic constitutive (E_M = 2.22 GPa and ν = 0.22 according to the benchmark values in Table 1). The quasi-brittle nature of masonry is represented by a linear type of softening in tension. In compression, a plateau exists after the compressive strength, followed by a linear type of softening. Damage variables are adopted when softening is active and aim at reducing the initial (undamaged) elastic modulus through the following equations:

$$\sigma_c = (1 - d_c)E_M\left(\varepsilon_c - \varepsilon_c^{pl}\right) \quad (1)$$

$$\sigma_t = (1 - d_t)E_M(\varepsilon_t - \varepsilon_t^{pl})$$

Where E_M is the elastic modulus of the undamaged masonry, σ_i is the current stress; d_i is the damage variable, ε_i is the total strain, and ε_i^{pl} is the plastic strain. The subscript i reads as c or t if associated with the compressive or tensile regime, respectively. To account for crushing and mixed failure modes, the compressive strength and the tensile strength of the units ($f_{t,b}$) complement the characterisation of the uniaxial stress-strain curves, which are detailed in Table 2. Moreover, a non-associative flow rule is employed to consider dilatancy and define the plastic strain rate, while a multiple-hardening Drucker-Prager type surface is used as the yield surface (Table 3).

Table 2: Compressive and Tensile stress-strain relationships

Compressive behaviour		
Stress [MPa]	Inelastic strain	d_c
3.96	0	0
3.96	0.008	0
0.1	0.04	0.9
Tensile behaviour		
Stress [MPa]	Inelastic strain	d_c
0.15	0	0
0.01	0.003	0.9

Table 3: Drucker-Prager strength domain parameters

Dilatation angle	Eccentricity	*fb,0 / fc,0*	*Kc*	Viscosity parameter
10°	0.1	1.16	2/3	1e-7

Structural model abstractions that account for the influence of the timber lintel and the interaction with the foundation led to the definition of three sub-grades within MR2 with a decreasing refinement: MR2.1) presence of lintel and concrete beams at the base of the piers (Figure 3 (a)); MR2.2) presence of lintel and absence of concrete beams at the base of the piers (Figure 3 (b)); MR2.3) absence of lintel and concrete beams at the base of the piers (Figure 3 (c)). Specifically, the timber lintel is modelled as a linear elastic isotropic material with an elastic modulus of 0.3 GPa, a Poisson's ratio of 0.2, and a density of 500 kg/m³. Additionally, the contact interfaces between the lintel and masonry, as well as between the structure and foundation, are modelled using friction-cohesive interfaces to allow potential detachment of the parts involved in the structural model.

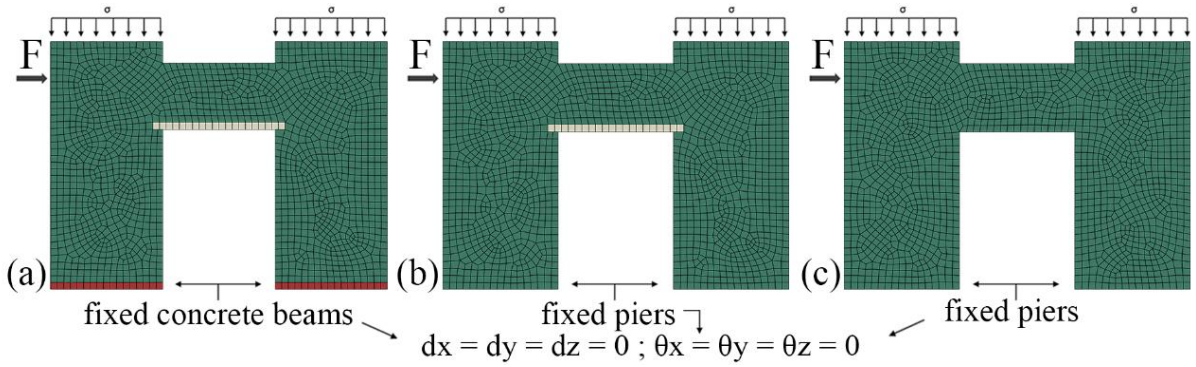

Figure 3: MR2 – Finite Element Modelling: (a) MR2.1; (b) MR2.2; (c) MR2.3

The three-dimensional FE model enforces the use of solid elements; therefore, the mesh discretisation is achieved using 20 nodes C3D20R hexahedral FEs with quadratic interpolation. Furthermore, appropriate boundary and loading conditions are implemented to perform the quasi-static analysis structural simulations according to the experimental setup [6], [7]. Figure 3 represents the three considered modelling abstractions and the mesh discretisation adopted.

4.3 Micro Limit Analysis (MR3)

Mi-LA formulation accounts for the unit-by-unit description of the masonry structure with the introduction of cohesive-frictional interfaces that represent masonry joints (Figure 4 (b)). In this approach, the masonry structure is composed of an assemblage of undeformable units, and no block penetration is admissible at the interfaces.

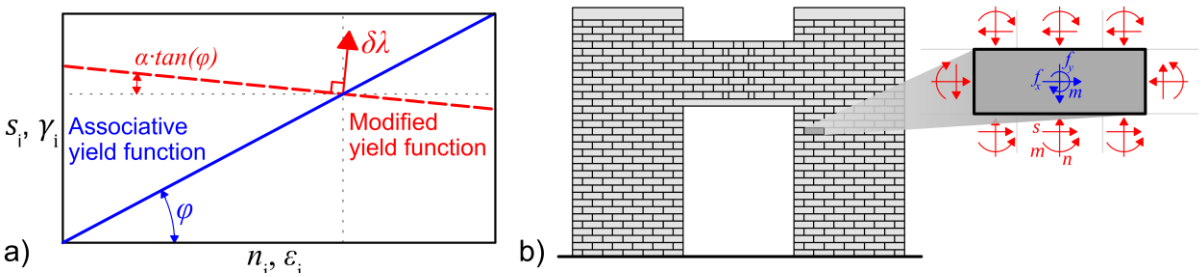

Figure 4: MR3 – Micro Limit Analysis: (a) Modification of yield function for the non-associative solution; (b) Masonry wall geometry and interface forces

In this work, the solution scheme proposed in [18] is adopted, where the sequential solution of linear programs solves the non-associative limit analysis problem. At each iteration, a linear program is defined by the following equation:

$$\begin{aligned} &\text{Maximise} \quad \lambda \\ &\text{Subject to} \quad \boldsymbol{Bq} - \lambda \boldsymbol{f}_L = \boldsymbol{f}_D \\ &\boldsymbol{C}^T[\boldsymbol{q} - \boldsymbol{c}] \leq 0 \end{aligned} \tag{2}$$

Where **q** is the vector of unknown contact forces, $\mathbf{f}_L$ and $\mathbf{f}_D$ are the live and dead loads, **c** is the cohesion vector, **B** and **C** are the equilibrium and yield constraint matrices, respectively. Finally, λ is the load factor, whose maximisation is the aim of the static limit analysis theorem. In the above equation, the two constraints represent the equilibrium of forces and the condition of interface failure.

To reach the non-associative solution, the yield conditions are updated at each iteration based on the interface normal forces at the previous iterations (Figure 4 (a)):

$$\begin{aligned} v_{i,j} &\leq c_i + \alpha \cdot \mu_i \cdot n_{i,j} \\ c_{i,j+1} &= c_i^0 + (1+\alpha) \cdot \left(\beta \cdot n_{i,j} + (1-\beta) \cdot n_{i,j-1}\right) \cdot tan(\varphi_i) \end{aligned} \tag{3}$$

Where $v_{i,j}$, $n_{i,j}$ and $c_{i,j}$ are the shear and normal forces and the cohesion of the *i-th* interface at the *j-th* iteration of the algorithm, while φ is the friction angle. Moreover, α and β algorithm parameters are set to 0.01 and 0.6, respectively. The algorithm procedure is not reported for the sake of brevity, and the reader can refer to [19].

4.4 Macro Limit Analysis (MR4)

LA remains a practical tool for assessing URM structures. The use of the Lower-Bound (LB) and Upper-Bound (UB) theorems has been interpreted as sub-grades of refinement within the LA method. Further sub-grades depend on the assumption of compressive strength (f_c). Therefore, four sub-grades have been considered: MR4.1) UB - finite f_c; MR4.2) UB - infinite f_c; MR4.3) LB - finite f_c; MR4.4) LB - infinite f_c. Computational thrust line analysis (CTLA) uses the LB theorem. Usually, this approach assumes infinite compressive strength, no tensile strength, and no shear failure, aiming to find a thrust line fully contained within the structure's boundaries to ensure structural equilibrium (MR4.4). However, since masonry has limited compressive strength, the thrust line cannot be tangent to the boundaries, and the model assumptions must be adjusted to prevent material crushing (MR4.3). To address this, the thrust line must maintain a distance ($d > t_h$ in Figure 5 (a)) from the external boundaries, calculated based on the wall's compressive strength and geometry, ensuring structural stability while avoiding crushing at critical points, as highlighted in [17], where details about the solutions algorithm are also provided.

On the other hand, the macro-block approach, which uses the UB theorem, can also be applied to assess the load factor causing the collapse of predefined macro-blocks that interact via hinges (Figure 5 (b,c)). This can be achieved by using different hypotheses, such as assuming either infinite (b) or finite (c) compressive strength in masonry. For infinite compressive strength (MR4.2), hinges form at the corners of piers in contact with the ground, while finite compressive strength (MR4.1) requires adjusting hinge positions based on the

resultant compressive stress. Internal hinges are also considered, accounting for masonry crushing. Once failure mechanisms and hinge positions are identified, equilibrium is defined using virtual displacement diagrams and solved for the horizontal force (F). Details about the solution procedure and algorithm implementation are reported in [14], [15].

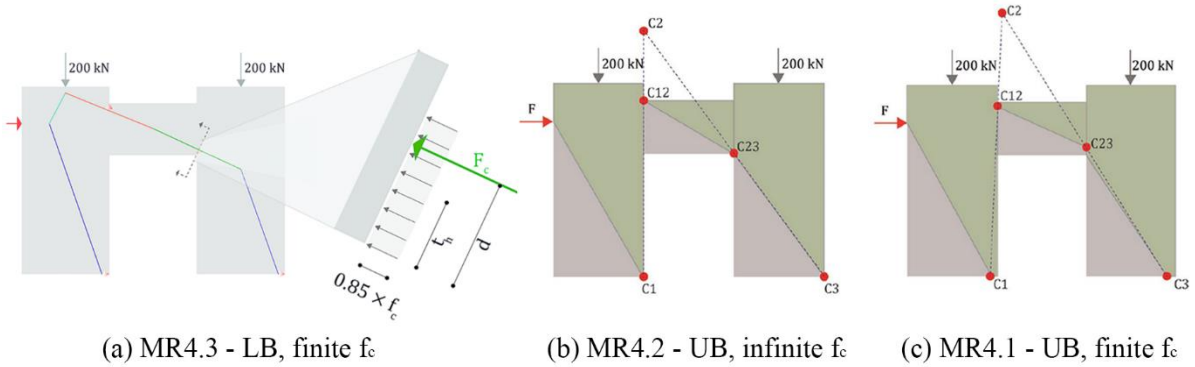

Figure 5: MR4 – Macro Limit Analysis: (a) MR4.3 LB approach with the hypothesis of finite f_c; (b) UB approach with the hypothesis of infinite f_c; (c) UB approach with the hypothesis of infinite f_c [15]

5 RESULTS AND DISCUSSION

This section presents the outcomes of each computational model and critically compares the four Modelling Refinements (MRs). In Figure 6, results for MR1 and MR2 correspond to a lateral displacement of 30 mm, approximately 1% drift, consistent with the experiment.

For MR1, the D-RBA-NCS model (Figure 6, MR1.1) aligns with the experimental test and SPA results, showing a diagonal tensile crack in the spandrel and piers' rocking mechanism. However, the MR1.1 model exhibits less ductility compared to SPA, as shown by the horizontal force-displacement curves in Figure 6 (b) and by modelling assumptions. For RD-RBA (Figure 6, MR1.2), the result related to one of the six mechanisms investigated is shown, representative of the failure mechanism characterised by damage concentration in the spandrel. No significant difference in ultimate lateral load is observed across the six collapse mechanisms investigated, as seen by comparing the minimum and maximum values given in Figure 6 (c) (Coefficient of Variation = 4%). In MR2 (FEM, Figure 6), more accurate boundary conditions and the inclusion of a lintel (MR2.1) influence the system's response, modifying both piers' response and spandrel damage. Although the maximum horizontal load is similar across MR2.1 to MR2.3, ductility decreases, with lower displacement values corresponding to the maximum horizontal force (Figure 6 (b)). The Mi-LA approach (Figure 6, MR3) fails to capture the pier-spandrel collapse mechanism due to the absence of a deformable lintel, and results in a higher maximum lateral load compared to other methods. Lastly, in Ma-LA, the maximum horizontal loads from LB and UB agree well, satisfying the uniqueness theorem. The refinement achieved by adopting the limited compressive strength and modified hinge positions at the spandrel (MR4.1 and MR4.3), provides a good match with the benchmark results. Comparing horizontal capacity, MR1 (DEM) is slightly conservative relative to the experimental test, while MR2 (FEM) better approximates the experimental maximum horizontal load. The infinite compressive strength assumption in Ma-LA (MR4.2 and MR4.4) and MR3 hypotheses overestimate lateral capacity, emphasising the importance of considering crushing in this masonry system.

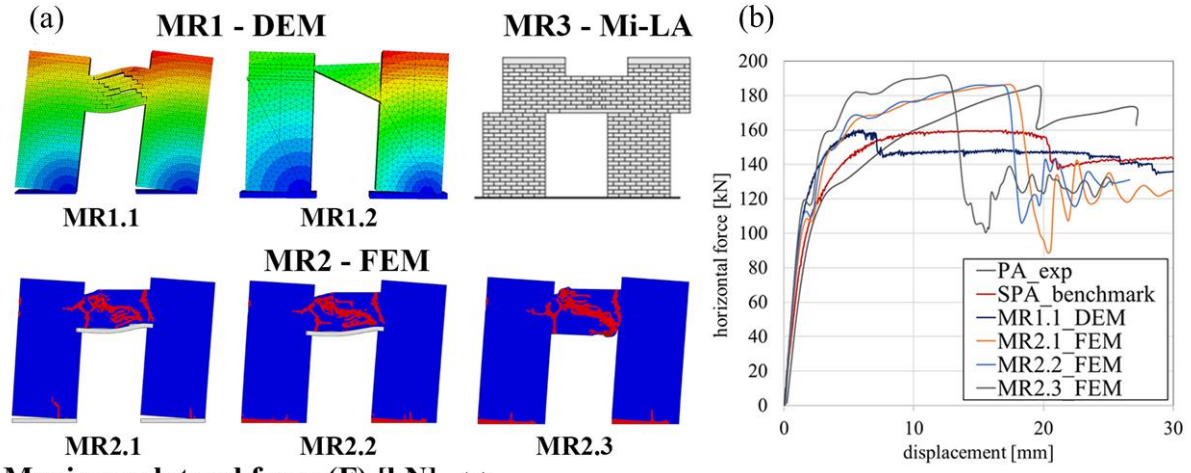

Maximum lateral force (F) [kN] (c)

PA	SPA	MR1		MR2			mi-LA	MR4			
		MR1.1	MR1.2	MR2.1	MR2.2	MR2.3		MR4.1	MR4.2	MR4.3	MR4.4
185	160	160	166 - 182.6	186.4	186.1	191.95	280	163.5	224.5	163	221.1

Figure 6: Outcomes of the four MRs; (a) Collapse mechanisms for MR1, MR2 and MR3; (b) Horizontal force-displacement curves for PA, SPA, MR1 and MR2; (c) Maximum lateral force for all MRs

Notably, as the MR is refined from more to less detailed, the required LoI decreases—not in terms of information quality (the mechanical parameters remain consistent with the 'real' ones discarding any mechanical uncertainty) but in quantity (less information is needed for less refined models). Essentially, elements are progressively removed from the initial SPA dataset (Table 1) as moving from MR1 to MR4 (Table 4). On the other hand, a reduction of the outcomes obtainable from the different MRs occurs (Figure 6).

Table 4: Comparison of the parameters needed to implement each modelling approach

		BLOCKS											MASONRY															
		E_b	G_b	f_{tb}	$k_{n,b}$	$k_{s,b}$	c_b	$\varphi_{0,b}$	$\varphi_{res,b}$	G^I_{fb}	G^{II}_{fb}	w_M	ν	E_M	G_M	$k_{n,j}$	$k_{s,j}$	$f_{t,j}$	$c_{0,j}$	$c_{res,j}$	$\varphi_{0,j}$	$\varphi_{res,j}$	f_c	G^I_f	G^{II}_f	G_c	**tot.**
	SPA - BM	x	x	x	x	x	x	x	x	x	x	x	x	x	x	x	x	x	x	x	x	x	x	x	x	x	**25**
MR1 - DEM	MR1.1 - D-RBA-NCS											x	x	x	x	x	x	x	x	x	x	x	x	x	x	x	**15**
	MR1.2 - RD-RBA											x	x	x		x							x			x	**6**
MR2 - FEM	MR2.1											x	x	x	x			x					x	x		x	**8**
	MR2.2											x	x	x	x			x					x	x		x	**8**
	MR2.3											x	x	x	x			x					x	x		x	**8**
MR3 - Mi-LA												x	x					x	x								**4**
MR4 - Ma-LA												x											x				**2 (1)**

6 CONCLUSION AND FUTURE WORK

This study proposes a framework for the rational implementation of digital models for monitoring and accurate prediction of structural performance loss of heritage masonry structures

The initial steps of the framework have been performed by investigating a structural benchmark taken from the literature. By implementing various computational approaches, the framework aims to demonstrate its ability to balance accuracy with computational efficiency. The numerical results only focus on the differences in computational approaches, highlighting

that even simplified computational approaches, if properly calibrated, offer competitive results at a lower computational cost. Future work will involve formulating and solving an optimisation problem to identify the most effective combination of modelling refinement and level of information. This will ensure the development of an 'optimal DT' under given scenarios, enhancing its practical applicability in heritage conservation.

REFERENCES

[1] "Joint Programming Initiative on Cultural Heritage and Global Change - Strategic Research and Innovation Agenda," 2020.

[2] M. Grieves and J. Vickers, *Digital Twin: Mitigating Unpredictable, Undesirable Emergent Behavior in Complex Systems*, no. August 2017. Springer, Cham, 2016. doi: 10.1007/978-3-319-38756-7.

[3] M. Grieves, "Digital Model , Digital Shadow , and Digital Twin," no. April, 2023.

[4] A. Vuoto, M. F. Funari, and P. B. Lourenço, "Shaping Digital Twin Concept for Built Cultural Heritage Conservation: A Systematic Literature Review," *Int. J. Archit. Herit.*, pp. 1–34, Sep. 2023, doi: 10.1080/15583058.2023.2258084.

[5] A. Vuoto, M. F. Funari, and P. B. Lourenço, "On the Use of the Digital Twin Concept for the Structural Integrity Protection of Architectural Heritage," *Infrastructures*, vol. 8, no. 5, p. 86, 2023.

[6] F. Parisi, N. Augenti, and A. Prota, "Implications of the spandrel type on the lateral behavior of unreinforced masonry walls Fulvio," *Pacific Conf. Earthq. Eng.*, no. 056, pp. 1–6, 2007, doi: 10.1002/eqe.

[7] N. Augenti, F. Parisi, A. Prota, and G. Manfredi, "In-Plane Lateral Response of a Full-Scale Masonry Subassemblage with and without an Inorganic Matrix-Grid Strengthening System," *J. Compos. Constr.*, vol. 15, no. 4, pp. 578–590, 2011, doi: 10.1061/(asce)cc.1943-5614.0000193.

[8] B. Pulatsu *et al.*, "Probabilistic approach to assess URM walls with openings using discrete rigid block analysis (D-RBA)," *J. Build. Eng.*, vol. 61, p. 105269, Dec. 2022.

[9] N. Augenti and F. Parisi, "Constitutive Models for Tuff Masonry under uniaxial compression," no. November, pp. 1102–1111, 2010.

[10] N. Augenti and F. Parisi, "Constitutive modelling of tuff masonry in direct shear," vol. i, pp. 1612–1620, 2011, doi: 10.1016/j.conbuildmat.2010.10.002.

[11] P. Cundall, "UDEC-A generalised distinct element program for modelling jointed rock," 1980.

[12] P. A. Cundall, "Formulation of a three-dimensional distinct element model-Part I. A scheme to detect and represent contacts in a system composed of many polyhedral blocks," *Int. J. Rock Mech. Min. Sci.*, vol. 25, no. 3, pp. 107–116, 1988, doi: 10.1016/0148-9062(88)92293-0.

[13] O. Cundall, PA., Strack, "A discrete numerical model for granular assemblies," *Geotechnique*, vol. 29, no. 1, pp. 47–65, 1979.

[14] B. Pulatsu, M. F. Funari, D. Malomo, S. Gonen, and F. Parisi, "Seismic assessment of URM pier spandrel systems via efficient computational modeling strategies," pp. 1–3, 2023.

[15] B. Pulatsu, S. Gonen, M. F. Funari, and F. Parisi, "Spatial stochastic D-RBA and limit equilibrium analysis of unreinforced masonry pier-spandrel structures," *Eng. Struct.*, vol. 296, no. September, p. 116897, 2023, doi: 10.1016/j.engstruct.2023.116897.

[16] G. Fortunato, M. F. Funari, and P. Lonetti, "Survey and seismic vulnerability assessment of the Baptistery of San Giovanni in Tumba (Italy)," *J. Cult. Herit.*, 2017, doi: 10.1016/j.culher.2017.01.010.

[17] S. Karimzadeh, M. F. Funari, S. Szabó, S. S. M. Hussaini, R. Sanaz, and P. B. Lourenço, "Stochastic simulation of earthquake ground motions for the seismic assessment of monumental masonry structures : Source-based vs site-based approaches," no. March 2023, pp. 303–330, 2024, doi: 10.1002/eqe.4012.

[18] M. Gilbert, C. Casapulla, and H. M. Ahmed, "Limit analysis of masonry block structures with non-associative frictional joints using linear programming," *Comput. Struct.*, vol. 84, no. 13–14, pp. 873–887, May 2006, doi: 10.1016/j.compstruc.2006.02.005.

[19] S. Szabó, M. F. Funari, B. Pulatsu, and P. B. Lourenço, "Lateral Capacity of URM Walls: A Parametric Study Using Macro and Micro Limit Analysis Predictions," *Appl. Sci.*, vol. 12, no. 21, Nov. 2022, doi: 10.3390/app122110834.